This is a previous version of the article published in Engineering Structures. 2021, 226: 111343. https://doi.org/10.1016/j.engstruct.2020.111343

In-plane shear cyclic behavior of windowed masonry walls reinforced with Textile Reinforced Mortars

Salvador Ivorra [1]*, Benjamín Torres[1], F. Javier Baeza[1] and David Bru[1]

[1] Department of Civil Engineering, University of Alicante. San Vicente Del Raspeig, Apartado 99, 03080, Spain

** Corresponding author. Tel.: +34 965903707; Fax: +34 96 590 3678. E-mail: sivorra@ua.es*

ABSTRACT

The current experimental study is focused on the mechanical performance of masonry walls under in-plane cyclic shear forces. All specimens were fabricated with a central window, in which the geometry considered the recommendations of the Spanish structural seismic design code. Windows represent a weak area in the masonry structure, in which there are stress concentrations responsible for crack initiation. In order to improve the mechanical strength and ductility, a reinforcement with a Textile Reinforced Mortar (TRM) was used on both sides of the wall. The performance of the unreinforced and reinforced masonry has been discussed in terms of strength and ductility gain, stiffness degradation and energy dissipation capacity. The experimental tests comprised an initial vertical preload, and shear cycles with increasing amplitude. All tests were monitored by means of traditional displacement transducers, and digital image correlation. The analysis of the images showed the time evolution of the overall crack distribution. The TRM effect could be observed as an increase of the mechanical strength (maximum shear from 120 kN to more than 300 kN), higher displacements (drift from 9 to 35 mm), and more energy dissipation (the cumulative energy loss from 2.7 to 12.7 kN·m). In addition, the TRM reinforcements were capable of controlling the crack initiation and growth. The widespread crack along mortar joints observed in the

unreinforced masonry became localized cracks (from the window's corners mainly), in which crack growth direction was not determined by masonry joints.

Keywords: Cyclic loads; masonry; Textile Reinforced Mortar (TRM); Fiber Reinforced Cementitious Matrix (FRCM); Digital Image Correlation (DIC).

1. Introduction

Masonry buildings are a traditional structural system, which can be found today as the constructive solution for new buildings or as heritage constructions, sometimes in seismic areas [1,2]. However, these structures usually present high seismic vulnerability due to their low tensile strength and the lack of reinforcement materials [3,4]. In particular, the most popular masonry structural system is the masonry wall, and it shows different behavior under in-plane or out-plane loads [5]. The seismic performance of masonry walls can be evaluated by means of their in-plane shear behavior, in which the usual failure modes are toe crushing, sliding, rocking and diagonal cracking [6,7].

Different external reinforcements can be used in order to reduce the seismic vulnerability of unreinforced masonry walls (URM) [8], for example composite materials, such as fiber reinforced polymers (FRP) [9,10]. The interest in these FRP solutions is focused on their low influence in the structural dynamic properties in addition to the mechanical capacity improvement, and both of them with a negligible increment of the structure's weight. However, FRPs also present some drawbacks related to high temperature exposure, FRP-masonry bonding in wet surfaces, or water permeability problems. Stratford et al. [11] presented some results of in-plane cyclic load tests, in which the FRP modified the crack patterns of masonry walls, but the FRP reinforced walls showed some FRP-masonry delamination. Different European laboratories have addressed this delamination issues by means of changing the resin matrix for another polyurethane based with five different types of reinforcement materials (glass, basalt, carbon or steel composites) [12].

Recently, Textile Reinforced Mortars (TRM) appeared as an alternative for the seismic retrofitting of URM walls [13,14]. These materials comprise a fiber mesh (glass, carbon or basalt) and a cement mortar with different additives for higher ductility. The main advantage of TRM is a better compatibility with masonry, which could avoid the aforementioned bonding or permeability issues. In addition, TRM can also improve masonry's strength and ductility [13]. Nevertheless, the efficiency of all these external reinforcements relays on the strain compatibility between all the elements involved (masonry substrate, matrix and fiber mesh), typical TRM failure comprise debonding or fiber slippage [15], hence specific measures should be taken to test the bonding compatibility of each particular solution [16].

For the seismic vulnerability of masonry wall structures, the key variables are their cyclic behavior, the stiffness' variation and energy dissipation, besides the mechanical properties of the material itself [17]. The effectiveness of TRM on these properties has been assessed in small masonry specimens [18] or full-scale masonry walls [19]. For example, TRM seemed to provide a significant improvement of masonry's strength and deformability [18]. However, in terms of strength gain, TRM solutions presented less efficiency, 65-70%, with respect to similar configurations made in FRP. Nonetheless, TRM was more effective than FRP for deformability enhancement, about 15-30% higher. Another study reported the effect of a continuous reinforcement in masonry's in-plane shear response [20]. TRM could effectively prevent diagonal cracks and shear failure, and the problems of masonry elements reinforced with FRP could be avoided.

The main objective of the current study is the evaluation of a TRM reinforcement for the purpose of seismic performance enhancement of masonry walls. There are several studies regarding the in-plane shear behavior of massive masonry walls, in which different dimensions and vertical preloads are combined [19,21]. However, there is less information regarding TRM solutions in walls with different openings, which represent weak elements in masonry structures. Therefore, the objective of this research was aimed at the evaluation of the cyclic behavior of unreinforced and reinforced masonry windowed walls. Their performance has been discussed in terms of strength and ductility gain, stiffness degradation and energy dissipation capacity. Finally, the influence of TRM on crack development, generated by in-plane shear cycles, was monitored by means of traditional displacement transducers and Digital Image Correlation (DIC) analysis. DIC technique has been applied to control crack location and growth along the whole surface of specimens [22].

2. Materials and methods

In this research two brick masonry walls were fabricated and tested under in-plane cyclic loads to assess their behavior in case of seismic events. One of them was previously reinforced with TRM to evaluate its reinforcement capacity. Fig. 1.a shows the general geometry of the masonry walls. Their dimensions (length x height x thickness) were 3x2x0.24 m, and presented a central window of 1x0.8 m. The window was constructed with an upper lintel, 1.5 m long, composed by three timber beams with a 150 x 75 mm^2 cross section. This geometry was designed according to the recommendations in the Spanish seismic structural design code NCSE-02 [23]. Masonry was fabricated with clay bricks and lime mortar. The brick's dimensions were 230x110x55 mm, and had 15 MPa compressive strength and 1550 kg/m^3 density (according to the supplier). The compressive strength of the lime mortar of the joints was measured in six 4x4x16cm^3 specimens, for a 120 days value of 9.2 MPa (± 6.8%), it should have a compressive strength >7.5 MPa according to the supplier.

In order to improve the wall's behavior under cyclic loads a Textile Reinforced Mortar (TRM) layer was applied to both 3x2 m^2 surfaces. This TRM was made with a Glass Fiber Mesh (see main properties in Table 1) in a fiber reinforced mortar (56 days compressive strength of 14.1 MPa ± 1.7%). Two orientations were combined in the reinforcement as defined in Fig. 2. The whole surface was reinforced with a continuous mesh oriented in the wall's main directions (0°-90°), while the four corners, where cracks were expected, counted with an additional mesh in the tensile stress principal direction (±45°). 20 cm overlaps were considered between two meshes in the same orientation.

Fig. 3 includes a general view of two tested specimens with all the auxiliary elements to apply the vertical preload and the lateral in-plane cyclic force. The experimental set up is shown in Fig. 1(b) and (c), in which horizontal loads were applied to point D using a hydraulic loading cell with a maximum capacity of 750 kN. A vertical load (150 kN) was applied using four Dywidag 32 before the beginning of the tests to simulate the weight of a three stories high building. Each Dywidag was monitored with a strain gage, in order to control the vertical preload of the test, and register the possible variability of the vertical load when lateral forces were applied. Different steel beams and cylinders were used to allow different displacements between the wall's drift and the upper loading devices. The shear force transmission was made with two steel plates located at the left and right sides of the wall, points A and D in Fig. 1(c), both of which were connected by four steel bars (ϕ20). These bars did not work in push cycles, as the force was directly applied to point D. However, in pull cycles, load was transferred to point A, and the bars were tensioned. Therefore, the displacement of the actuator that controlled the loading rate and cycle’s amplitude included the elongation of the tensioned bars. This difference between push and pull cycles was the reason of the asymmetry in the wall’s behavior, as will be shown in the discussion section. Moreover, no specific measures were taken to avoid the rotation of the head of the wall during the test. Therefore, the unreinforced wall may have experienced some flexural effect, causing the crack initiation near the base, as will be discussed in detail later. The displacement rate was fixed during the whole test and the drift amplitude was progressively increased. Each amplitude was repeated once before passing to the next loading step.

Four LVDTs were attached to the structure to register crack openings, and horizontal displacements (in the base, B, and the top, D). The opposite side was monitored with a Digital Image Correlation (DIC) system. DIC is a non-contact optical technique used for measuring strain and displacement [24]. The position of each object point in the image can be identified by applying a correlation algorithm using a stochastic intensity pattern (speckle) on the object surface. Using this technique, deflections, axial deformations, local strains and crack patterns can be determined. The resolution of the DIC is related to the pixel density of the camera, the size of the area of interest and the quality of the speckle.

For the current DIC measures, a 16 MP camera and the GOM Correlate software [25] were used. The software was used to process the images and obtain the field of displacements of one side of the wall. This system was previously tested on FRCM direct tensile tests and masonry wallets in diagonal tension tests[26]. Only one camera was used because the out-of-plane displacement is considered negligible compared to the in-plane components. A crucial step is the creation of the stochastic pattern (Fig. 4.a). In order to optimize the analysis, the perfect contrast in the images was improved by painting in white the walls before applying the black speckle [24]. Fig. 4.b shows the good agreement between DIC and LVDT systems in this study.

3. Results and discussion

Two windowed masonry walls were tested under in-plane cyclic loads to evaluate the efficiency of a TRM reinforcement as an alternative for the seismic reinforcement of masonry buildings. The following results have been analyzed considering several aspects such as ductility, properties' degradation or cracking evolution. Table 2 summarizes the main results of both specimens, which will be specifically discussed in each of the following subsections.

3.1 Hysteretic response

The mechanical behavior of the specimens was evaluated by the relationship between loads and the displacements of the upper part of the wall. In this case, displacements have been represented as the drift, i.e. the difference between the lateral movements of the upper and lower part of the wall. Figure 5 shows the hysteresis cycles for the specimens up to an interval displacement of -35 and 30 mm for a reinforced wall (TRM-W), and -9 and 9 mm for an unreinforced wall (U-W). The similarity and symmetry of the displacements in both directions should be pointed out here. The drift amplitudes in the unreinforced wall were lower. However, for a 9 mm drift the damage detected could compromise the overall stability. Hence, the incremental cycles were changed for pushover tests at the same constant displacement rate.

The initial response of both structures was similar, but the U-W rapidly degraded after cracks initiated. On the other hand, the TRM-W could still resist higher loads and displacements beyond the U-W failure. On average, the maximum loads reached by the TRM-W at the end of the test were 204% higher than their U-W counterparts (see Fig. 5). In addition, the TRM seemed to increase the energy dissipation capacity, which could be seen as a greater ductility.

3.2 Envelopes and mechanical performance

Fig. 6 shows the load vs drift envelope curves for both walls, considering the maximum response of each cycle. In this case, the change of the stiffness could be obtained as the load/drift ratio. Although U-W and TRM-W specimens had very different behavior, both specimens showed similar mechanical performance in both drift directions.

The unreinforced wall, U-W, could resist a maximum 120 kN load, and a -9 mm drift. Higher displacements produced a behavioral change. Specially, during the pushover cycles U-W specimen behaved as two independent structures because after a 9 mm push and pull a horizontal crack all along the wall's section had been generated. Therefore, both parts were detached, the upper mid wall continued moving, while the lower part remained still, hence the crack widened but the rest of the structure wasn't anymore damaged. For this reason, after a ± 9 mm drift, cycles were changed to pushover tests. The U-W envelope curve in Fig, 6, after -9 mm, shows that the load remained relatively constant with only a small increase (133 kN, 9.7 % of the failure load that was 120 kN) as the imposed drift increased. It could be due to overcoming the friction between the two wall sub-structures, which could increase due to restrains imposed by vertical load to avoid the separation of both parts of the wall. Finally, the drift at the end of the test was around -35 mm. After this first pushover test, another one in the pull direction was made with similar behavior. However, in this case there was a load increase with respect to the maximum values of 120 kN and 9 mm, which were reached during cyclic loading. This increase may have been due to overcoming the friction between both parts of the wall, but it may also be related to the wedge effect produced by the failure surface of the first push-over. In U-W specimen, failure occurs mainly in a surface following the mortar joints between bricks. Failure in push direction implied a stepped surface that gradually opened. However, when pushover was made in the contrary direction, this gap in the stepped surface closed again, increasing the strength of the wall and the load value.

On the other hand, specimen TRM-W showed maximum loads and drifts of 300 kN and -33 mm (push), and -360 kN and 30 mm (pull). These values prove the effect of the two TRM layers on the mechanical performance of the masonry wall, which can be summarized as follows:

- Both specimens presented linear behavior during the first load cycles. Besides, no damage occurred in this stage as confirmed by visual inspection. The TRM-W specimen presented a linear load/drift ratio in the interval of [-5, 8] mm. Beyond this point, the behavior became non-linear showing with more ductility than U-W specimen. On the other hand, the U-W specimen only showed linear behavior in the interval [-2, 2] mm, and the non-linear response was registered up to [-9, 9] mm.
- The general behavior of both specimens was similar for lower displacements (linear regime) but the non-linear and ductility response of each wall differed. As drifts increased, the U-W specimen did not present ductility, and the maximum load was around 133 kN and was used to overcome the friction between the two sub-structures. On the other hand, the TRM-W specimen

showed a strengthening behavior with more ductility than U-W after crack initiation. TRM performed correctly and mesh slippage or TRM debonding was not observed during the test.

- Despite the effect on the wall's strength, the TRM did not change the initial stiffness of the wall, for low drifts. The effect of the TRM in the stiffness degradation will be discussed below.

3.3 Energy dissipation capacity

The energy dissipated in a single load cycle (i.e. for a certain drift) was obtained using the trapezoid rule to assess the area within the hysteretic load-drift curve (Fig. 5). This energy loss has been represented in Fig. 7 as the dissipation of each cycle (Fig. 7.a and 7.b), or as the cumulative energy (Fig. 7.c).

In general, the cycles with the same drift did not dissipate equal energy. The second cycle dissipated less energy, as the main loss occurred when cracks appeared in the first cycle. In addition, the amount of energy was higher for wider cycle amplitudes (see Fig. 7.a and 7.b). Nevertheless, the U-W presented a reduction of energy loss between 7 and 8 mm drifts, see Fig. 7.b. This seemed to be a symptom of strength loss. Hence, the test was decided to be finished below this point.

As explained before, the unreinforced wall was damaged earlier. Therefore, for low levels of displacement, the U-W specimen was already cracked and dissipated more energy than the TRM-W. However, at the end of the test, considering the ductility of each sample, the TRM-W showed higher energy dissipation capacity, and the total energy loss was 529% with respect to the U-W (see Fig. 7.c). Thus, the TRM enhanced the behavior in terms of total energy dissipation and higher ductility, which could be observed as a delayed crack development, which may prove the TRM as a suitable solution to improve the behavior of masonry walls to cyclic loads. The specific crack patterns will be discussed with the DIC analysis.

3.4 Stiffness degradation

In order to assess the structural degradation, the stiffness *K* corresponding to a certain drift value was obtained as the secant stiffness at 70% of the maximum load of the cycle [20,27]. Stiffness was determined for both directions of displacement –push (-) and pull (+)–, all of which seemed to present similar degradation. Fig. 8 includes this stiffness change vs the drift of each cycle. For a better comparison, Fig. 8.b represents the stiffness as the residual value (i.e. with respect to the initial stiffness), or as the percentage of that initial stiffness that was lost after a certain drift. As confirmed by visual inspection, no damage occurred during the first elastic phase. Afterwards significant cracking appeared on the wall, as shown in the stiffness drop. Even though the initial stiffness –at low drifts– for both walls was similar, the stiffness of the U-W specimen was rapidly reduced as the damage level increased, while the TRM-W specimen preserved the mechanical response, showing a slower degradation. Therefore, the TRM can guarantee a better performance because for the same deformation of the wall, it presented less structural degradation. Actually, the U-W specimen suffered almost a linear loss from the beginning. After suffering 1 cm drifts the U-W specimen lost approximately 90% of its original stiffness. On the other hand, after the same drift was applied to the TRM-W specimen, the average loss was only 31%, i.e. when U-W had already failed TRM-W still had 69% of its original stiffness. In fact, after suffering displacements more than three times wider, [-35, 30] mm approximately, the TRM reinforcement was capable of still responding with 50 to 60% of its initial stiffness.

Fig. 9 presents the relationship between the energy dissipation and the stiffness degradation. The energy dissipation of each cycle (Fig. 9.a) or the cumulative energy up to a certain drift (Fig. 9.b) have been plotted vs the stiffness loss. In both graphs, the different behavior between both specimens can be observed. The U-W presented a linear increase of the energy dissipation as more damage was generated. However, the TRM-W registered an exponential growth of the energy loss per cycle (see Fig. 9.a). This trend of the TRM-W led to a practically bilinear function of the cumulative energy dissipation-stiffness loss curve (Fig. 9.b), in which a 50% stiffness loss seemed to be the transition point between the higher and lower dissipation phases. Despite the main effect of TRM was observed for big drifts, it could be seen even at small deflections when there was not still any damage. Fig. 9(a) includes regression analyses for both series, and the energy loss at 0% stiffness degradation were 36.6 kN·mm (U-W) and 97.9 kN·mm (TRM-W). Thus, even in an undamaged wall, the dissipation capacity of the TRM-W was 268% with respect to the U-W value.

3.5 Crack patterns: LVDT vs DIC

Finally, cracks were monitored with LVDTs located on one side near the window's corners and an additional DIC system was used to monitor the other side (to collect data from the whole wall). A comparison between the measures of both techniques was presented above (see Fig. 4).

Fig.10 includes the values registered in the LVDTs vs the shear load. Each graph includes the two sensors located in one diagonal direction or the other. Fig. 10 represents positive force values in the push direction (to the left), and negative ones in pull cycles (to the right). Push cycles generated compressions in LVDT1-2 and tensions in LVDT3-4, while pull cycle's behavior was reversed (tensions in LVDT1-2 and compressions in LVDT3-4). Therefore, compressions in Fig. 10 may be seen as negative deformations, while tensions are elongations (positive deformations).

Crack development may be seen as slope changes in the tension side of each curve. The U-W presented cracks in all four window's corners after the pushover tests. In this case, the maximum shear forces were between 150 and 200 kN, and the measured elongations almost reached 18 mm in the bottom corners, while were only 12 mm in the upper ones. Besides, LVDT2 showed more deformation than LVDT1 in the left direction, which was another evidence of the relative displacement as rigid bodies between the upper and lower parts, and the friction between both surfaces.

The TRM-W sample was capable of controlling the crack opening, and the maximum apertures (7.5 and 9.5 mm) were obtained at higher load values (300 kN and 360 kN). If both responses, U-W and TRM-W, are compared, the initial stiffness in both cases seemed to be similar. Damage was rapidly produced in the unreinforced wall, and the maximum capacity was reached even at low displacements. In addition, the TRM-W showed more mechanical capacity and progressive deterioration, with gradual stiffness loss in tension as loads increased and cracks developed. On the contrary, the TRM-W behavior in compression was linear during the whole tests. Therefore, the fiber mesh in the TRM served as a crack opening control element, improving the behavior of masonry wall structural members subjected to cyclic in-plane shear forces.

In order to evaluate the overall crack pattern, displacement evolution was monitored with digital images. Fig. 11 includes the results of the DIC analysis for the maximum drifts applied to each wall, in which red lines represent areas with tensile strain values higher than 1%. DIC images were taken on the opposite side of LVDT measures, hence, push cycles in Fig. 11 correspond to drifts to the right, and pull tests to the left (contrary to the criteria in Fig. 10). In Fig.11, the difference between both specimens was stronger. TRM-W showed a more controlled cracking, in which the ductile behavior was observed at higher shear forces despite all the distributed cracking. In both specimens, cracks initiated around the window corners, and developed following the diagonal direction. The U-W cracks developed along mortar joints, while TRM cracks were continuous. In the U-W, besides the widespread cracks highlighted in red in Fig. 11.b and 11.c, there was a wider horizontal crack in the lower part cutting the wall in two independent elements. This continuous crack -typical failure mode of masonry walls [28]- disconnected the two parts, both of which moved separately for the rest of push-over tests. This crack can be easily observed in Fig. 12, which shows the horizontal displacement distribution of the U-W at the end of both pushover cycles. In this case, the difference between both wall's subsections was clearly detected.

For future dynamic modelling of masonry structures, the equivalent viscous damping could be used to represent the energy dissipation capacity of the structure, and the stability of the hysteresis behavior. This equivalent damping ξ_{eq} can be defined by the ratio between the area of hysteresis cycles $S_{ABC} + S_{CDA}$ and the corresponding elastic energy $S_{OBE} + S_{ODF}$, according to eq. (1), and as shown in Fig. 13(a).

$$\xi_{eq} = \frac{1}{2\pi} \cdot \frac{S_{ABC} + S_{CDA}}{S_{OBE} + S_{ODF}} \tag{1}$$

Fig. 13(b) includes the values of ξ_{eq} for each cycle, shown as the damage level (i.e. stiffness loss). Both structures, showed a similar trend, in which damping was reduced as damage was being accumulated. The European seismic code [29] prescribes a damping ratio between 5 and 10% for masonry structures. The damping values of the reinforced wall were basically in that interval, only a few were slightly higher than 10%. However, the equivalent viscous damping values of the unreinforced wall were much higher than the recommended values in EC-8. At low displacements, damping values were almost 25%, but considering the fast degradation of the mechanical response, it may seem reasonable to adopt values closer to 10%, as those shown by the unreinforced wall after suffering severe damage. Nonetheless, according to the current results the U-W showed more equivalent damping than the TRM-W. Unreinforced masonry presented wider crack distribution along the whole structure, which may be responsible for the bigger damping. While the TRM prevented crack development, which were more localized around the corners. Hence, the fissure length (i.e. friction areas) was controlled, and the energy had to be accumulated in the TRM itself, as cracks in the mortar, or elastic energy in the fiber mesh.

4. Conclusions

The effectiveness of a TRM reinforcement in the in-plane cyclic behavior of windowed masonry walls was assessed. After the experimental tests, and the analyses of results in terms of strength, ductility, energy loss and stiffness degradation, the following conclusions may be drawn:

- When the wall was reinforced with TRM, the mechanical capacity of the wall was increased an average 204% with respect to the unreinforced masonry strength. Besides, the structural ductility was enhanced, as the maximum drifts increased from 9 mm to 35 mm due to the TRM reinforcement.
- The energy dissipation capacity for small drifts (< 1 cm) was higher in the unreinforced masonry. Nevertheless, this energy loss implied a faster structural degradation and widespread crack development. The higher ductility related to the TRM was also observed in the cumulative energy loss, which increased from 2.7 kN·m (unreinforced) up to 12.7 kN·m (with TRM).

- The initial stiffness was similar between the two structural solutions, 30 kN/mm approx. Hence, the effect of TRM seemed to be negligible in the elastic behavior. However, the damage in the unreinforced masonry led to residual stiffness below 10% of that initial value after only 9 mm drifts. While, the TRM guaranteed the structural stability, preserving at least 40% of the initial stiffness even after a 30 mm drift.
- Finally, the TRM layers also modified the cracking pattern. Unreinforced masonry showed distributed cracks along the whole surface, following joint directions. Even longitudinal crack in the low part affected the complete cross section, which produced a relative displacement between two independent sub-walls. The TRM was capable of controlling the crack initiation and growth. Main cracks were concentrated in the four window’s corners, and their direction did not follow the masonry joints.

Acknowledgements

The authors would like to acknowledge Mapei Spain S.A. for the materials supplied in this research. This research was funded by Spanish Ministry of Economy and Competitiveness, grant number BIA2015-69952-R and Spanish Ministry of Science, Innovation and Universities, grant number RTI2018-101148-B-I00.

References

[1] Bru D, Reynau R, Baeza FJ, Ivorra S. Structural damage evaluation of industrial masonry chimneys. Mater Struct 2018;[in Press].

[2] Diaferio M, Foti D. Seismic risk assessment of Trani’s Cathedral bell tower in Apulia, Italy. Int J Adv Struct Eng 2017;9:259–67. https://doi.org/10.1007/s40091-017-0162-0.

[3] Bru D, Ivorra S, Baeza FJ. Seismic behavior of a masonry chimney retrofitted with composite materials: A preliminary approach. Int J Saf Secur Eng 2017;7:486–97. https://doi.org/10.2495/SAFE-V7-N4-486-497.

[4] Endo Y, Pelà L, Roca P, da Porto F, Modena C. Comparison of seismic analysis methods applied to a historical church struck by 2009 L'Aquila earthquake. Bull Earthq Eng 2015;13:3749–78.

[5] Magenes G, Calvi GM. In-plane seismic response of brick masonry walls. Earthq Eng Struct Dyn 1996;26:1091–112.

[6] Reboul N, Mesticou Z, Si Larbi A, Ferrier E. Experimental study of the in-plane cyclic behaviour of masonry walls strengthened by composite materials. Constr Build Mater 2018;164:70–83.

[7] Endo Y, Pelà L, Roca P, da Porto F, Modena C. Comparison of seismic analysis methods applied to a historical church struck by 2009 L'Aquila earthquake. Bull Earthq Eng 2015;13:3749–78. https://doi.org/10.1007/s10518-015-9796-0.

[8] Bhattacharya S, Nayak S, Dutta SC. A critical review of retrofitting methods for unreinforced masonry structures. Int J Disaster Risk Reduct 2014;7:51–67.

[9] Zhang S, Yang D, Sheng Y, Garrity SW, Xu L. Numerical modelling of FRP-reinforced masonry walls under in-plane seismic loading. Constr Build Mater 2017;134:649–63.

[10] Triantafillou TC. Strengthening of masonry structures using epoxy-bonded FRP laminates. J Compos Constr 1998;2:96–104.

[11] Stratford T, Pascale G, Manfroni O, Bonfiglioli B. Shear Strengthening Masonry Panels with Sheet Glass-Fiber Reinforced Polymer. J Compos Constr 2004;8:434–43.

[12] Kwiecień A, de Felice G, Oliveira D V., Zając B, Bellini A, De Santis S, et al. Repair of composite-to-masonry bond using flexible matrix. Mater Struct Constr 2016. https://doi.org/10.1617/s11527-015-0668-5.

[13] Babatunde SA. Review of strengthening techniques for masonry using fiber reinforced polymers. Compos Struct 2017;161:246–55.

[14] Bernat E, Gil L, Roca P, Escrig C. Experimental and analytical study of TRM strengthened brickwork walls under eccentric compressive loading. Constr Build Mater 2013;44:35–47. https://doi.org/10.1016/j.conbuildmat.2013.03.006.

[15] Ceroni F, Salzano P. Design provisions for FRCM systems bonded to concrete and masonry elements. Compos Part B Eng 2018. https://doi.org/10.1016/j.compositesb.2018.01.033.

[16] de Felice G, Aiello MA, Caggegi C, Ceroni F, De Santis S, Garbin E, et al. Recommendation of RILEM Technical Committee 250-CSM: Test method for Textile Reinforced Mortar to substrate bond characterization. Mater Struct Constr 2018. https://doi.org/10.1617/s11527-018-1216-x.

[17] Tomazevic M, Lutman M. Seismic behavior of masonry walls: modeling of hysteretic rules. J Struct Eng 1996;122:1048–54.

[18] Papanicolaou CG, Triantafillou TC, Karlos K, Papathanasiou M. Textile-reinforced mortar (TRM) versus FRP as strengthening material of URM walls: in-plane cyclic loading. Mater Struct 2007;40:1081–97.

[19] Wu F, Wang H-T, Li G, Jia J-Q, Li H-N. Seismic performance of traditional adobe masonry walls subjected to in-plane cyclic loading. Mater Struct 2017;50:69.

[20] Deng M, Yang S. Cyclic testing of unreinforced masonry walls retrofitted with

engineered cementitious composites. Constr Build Mater 2018;177:395–408.

[21] Arêde A, Furtado A, Melo J, Rodrigues H, Varum H. Challenges and main features on quasi-static cyclic out-of-plane tests of full-scale infill masonry walls. 7th Int Conf Adv Exp Struct Eng 2017:373–88.

[22] Bilotta A, Ceroni F, Lignola GP, Prota A. Use of DIC technique for investigating the behaviour of FRCM materials for strengthening masonry elements. Compos Part B Eng 2017;129:251–70.

[23] NCSE-02. NCSE-02. Norma de construcción sismorresistente: parte general y edificación. 2004.

[24] Strauss A, Castillo P, Bergmeister K, Krug B, Wan-Wendner R, Marcon M, et al. Shear performance mechanism description using digital image correlation. Struct Eng Int 2018;28:338–46.

[25] Gom correlate. “https://WwwGomCom/3d-Software/Gom-CorrelateHtml” 2020.

[26] Torres B, Varona FB, Baeza FJ, Bru D, Ivorra S. Study on Retrofitted Masonry Elements under Shear Using Digital Image Correlation. Sensors 2020;20:2122. https://doi.org/10.3390/s20072122.

[27] Torres B, Bertolesi E, Calderón PA, Moragues JJ, Adam JM. A full-scale timbrel cross vault subjected to vertical cyclical displacements in one of its supports. Eng Struct 2019;183:791–804.

[28] Mahjoob Farshchi D, Motavalli M, Schumacher Empa A, Sadegh Marefat M. Numerical modelling of in-plane behaviour of URM walls and an investigation into the aspect ratio, vertical and horizontal post-tensioning and head joint as a parametric study. Arch Civ Mech Eng 2009;9:5–27.

[29] European Commitee for Standardization. Eurocode 8: Design of structures for

earthquake resistance - Part 1 : General rules, seismic actions and rules for buildings. Eur Comm Stand 2004;1.

Figure 1. (a) Geometry of masonry walls; Test characteristics (b) front elevation, (c) lateral view.

Figure 2. TRM reinforcement distribution, G220 oriented in 0°-90° and ±45° directions.

Figure 3. Tested walls: (a) Unreinforced, (b). TRM reinforced sample.

Figure 4. (a) DIC speckle in the TRM-W. (b) Comparison between DIC and LVDT.

Figure 5. Hysteretic load-drift curves.

Figure 6. Load-drift envelope curves.

Figure 7. Energy dissipation vs drift curves per cycle (a), magnification for displacement <1 cm (b), and cumulative energy dissipation (c).

Figure 8. Stiffness degradation: (a) Stiffness vs drift; (b) Relative stiffness K/K_o *and stiffness loss vs drift.*

Figure 9. Energy dissipation vs stiffness degradation: (a) cycle's energy loss vs stiffness loss; (b) cumulative energy vs stiffness loss.

Figure 10. Shear vs LVDT measures: (a) LVDT1 and LVDT2, (b) LVDT3 and LVDT4.

Figure 11. Crack analysis by DIC, for different drift values (red lines represent tensile strains >1%).

Figure 12. Horizontal displacements of the U-W by means of DIC corresponding to maximum drifts in (a) push and (b) pull directions.

Figure 13. (a) Equivalent viscous damping, and (b) its variation vs stiffness loss.

Table 1. Fiber mesh type properties (given by the supplier).

Material	Mesh size (mm)	Weight (g/m²)	Tensile strength (MPa)	Elongation at failure (%)	Elastic modulus (GPa)
Glass	25x25	225	1276	1.8	72

Table 2. Summary of the main results. Brackets show the values in [push, pull] directions.

Properties.	**U-W**	**TRM-W**
Displacements at failure (mm)	[-9, 9]	[-35, 30]
Maximum displacements during pushover test (mm)	[-36, 35]	-
Maximum loads (kN)	[133, -180]	[300, -360]
Displacements in elastic behavior (mm)	[-2, 2]	[-5, 8]
% Cumulative energy dissipation ${CED_{TRM-W}}/{CED_{U-W}}$	529	
Residual stiffness (%) at [-30, 30] mm	[1, 7]	[40, 50]
Stiffness loss (%) at [-30, 30] mm	[99, 93]	[60, 50]
Maximum crack width (mm) and position	18 mm in LVDT2 and LVDT3 for both push-pull direction	9.5 mm in LVDT2 for pull direction
Equivalent viscous damping (%)	25-10	10-5

Figure 1

Click here to access/download;Figure;Fig1.png

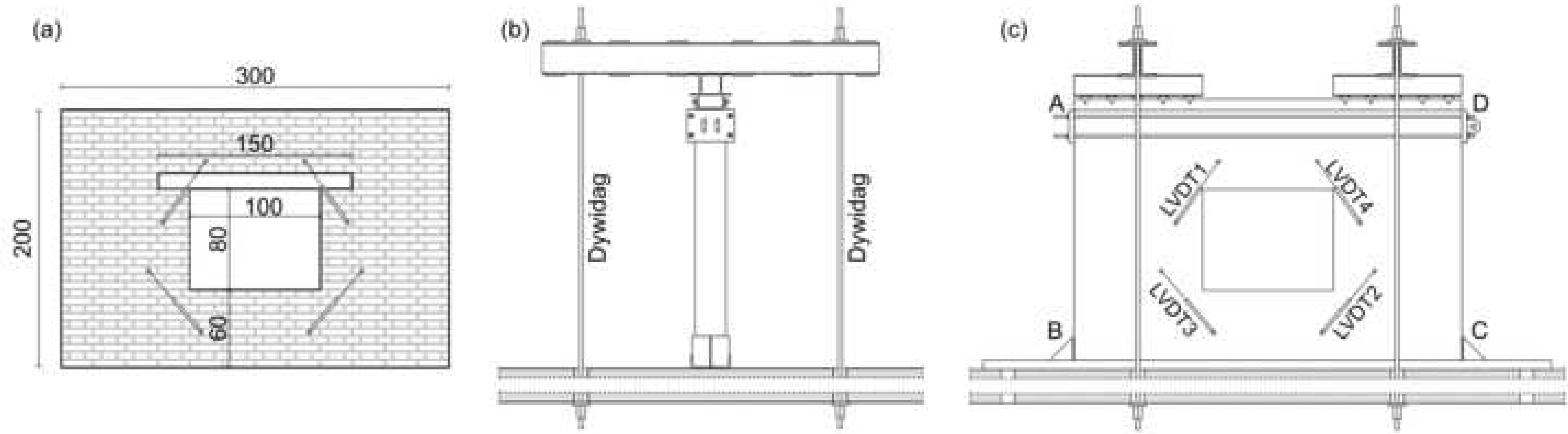

Figure 2

Click here to access/download;Figure;Fig2.png

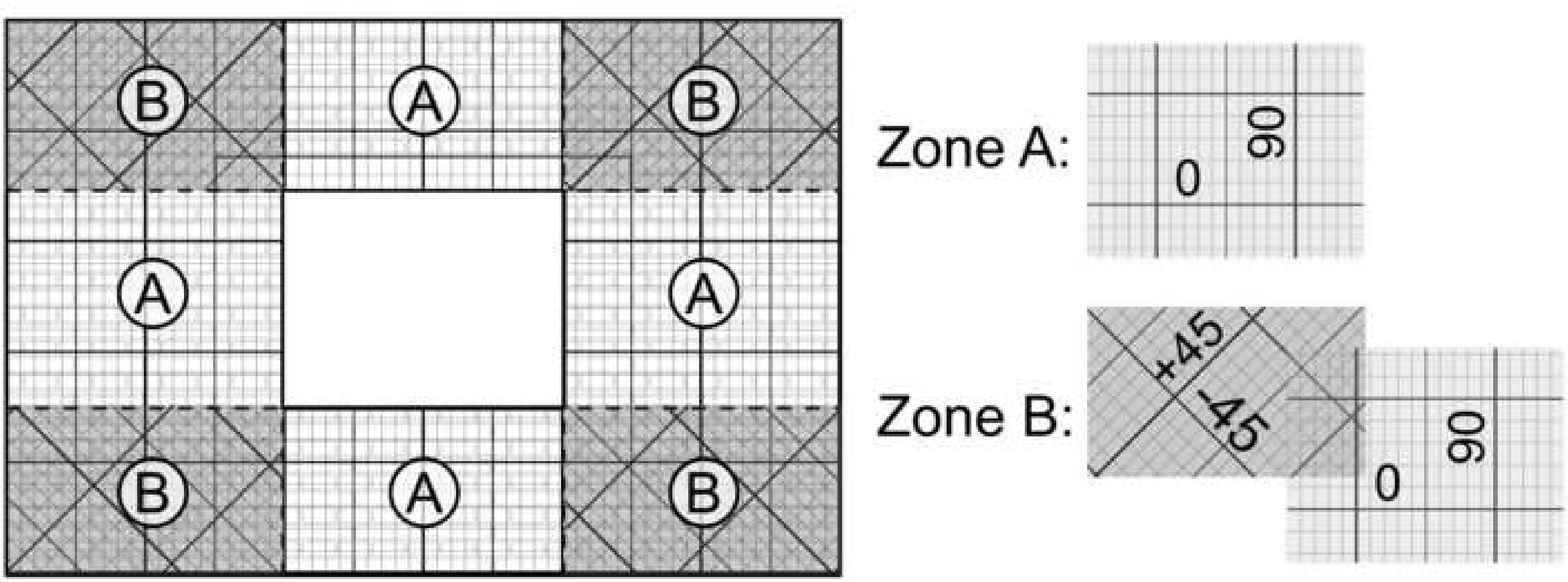

Figure 3

(a) Unreinforced wall, U-W (b) TRM reinforced wall, TRM-W

Figure 4

Click here to access/download;Figure;Fig4.tif

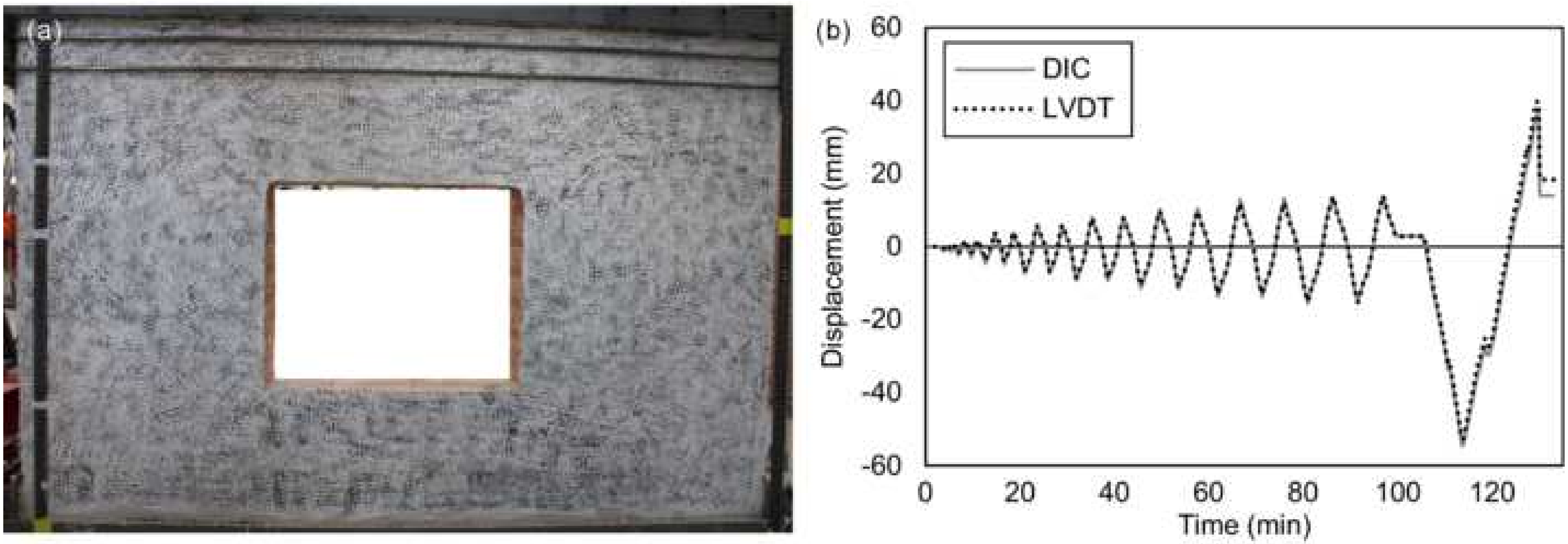

Figure 5

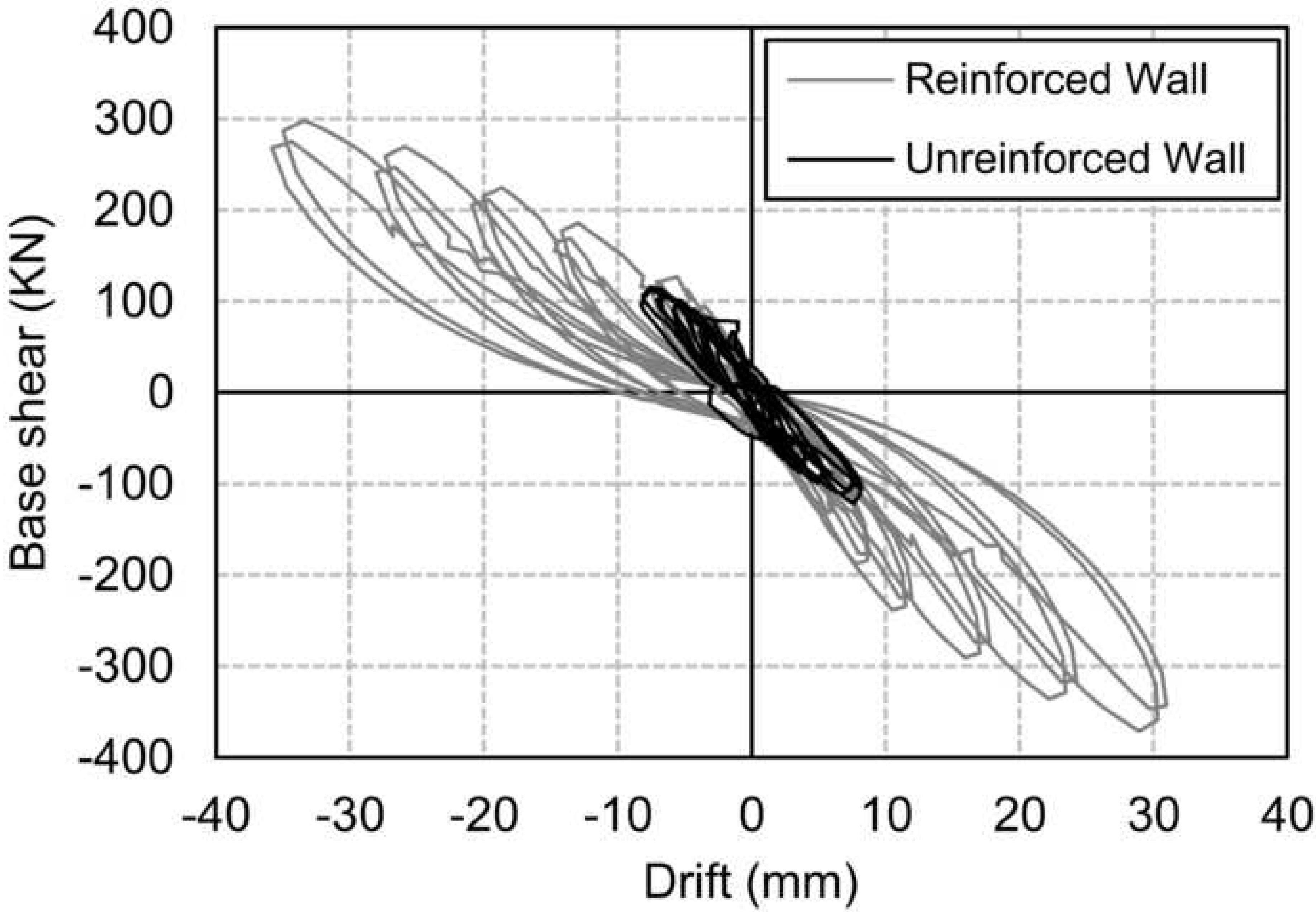
Reinforced Wall
Unreinforced Wall
Base shear (KN)
400
300
200
100
0
-100
-200
-300
-400
-40
-30
-20
-10
0
10
20
30
40
Drift (mm)

Figure 6 _ revised

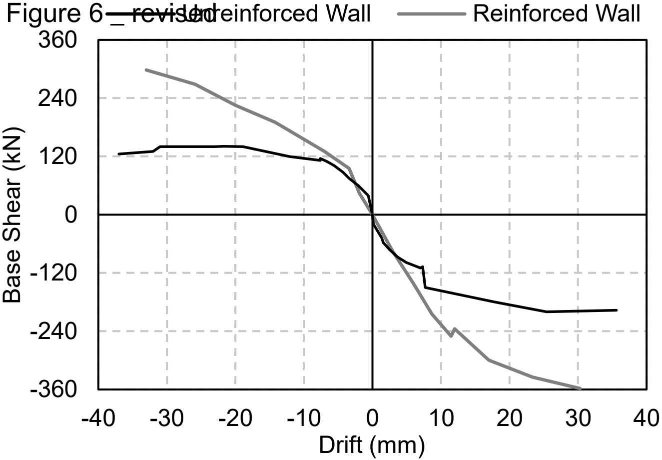

Figure 7_revised

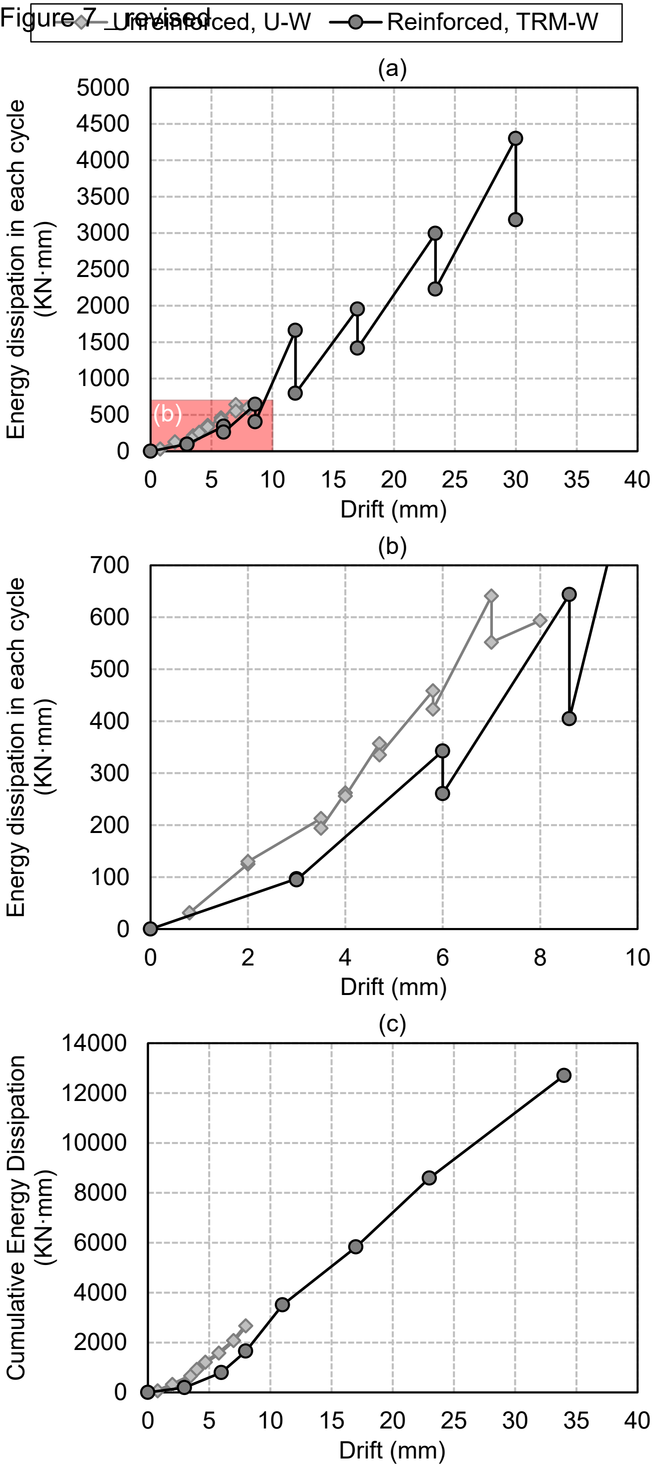

Figure 8

Click here to access/download;Figure;Fig8.png

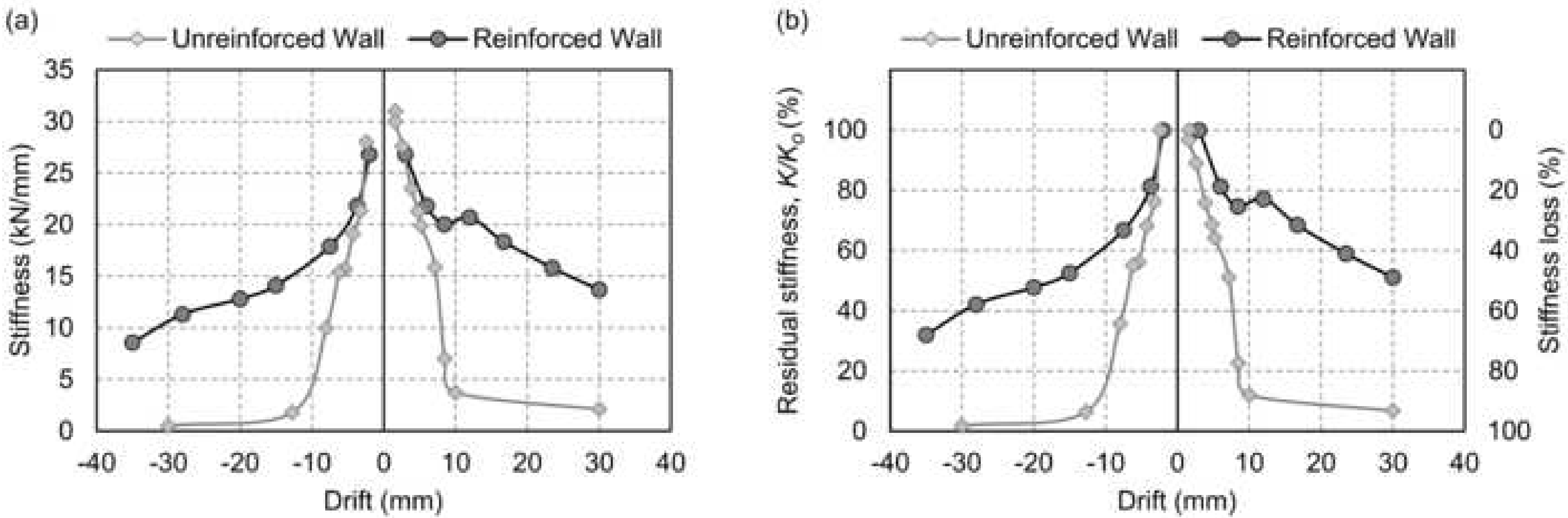

Figure 9

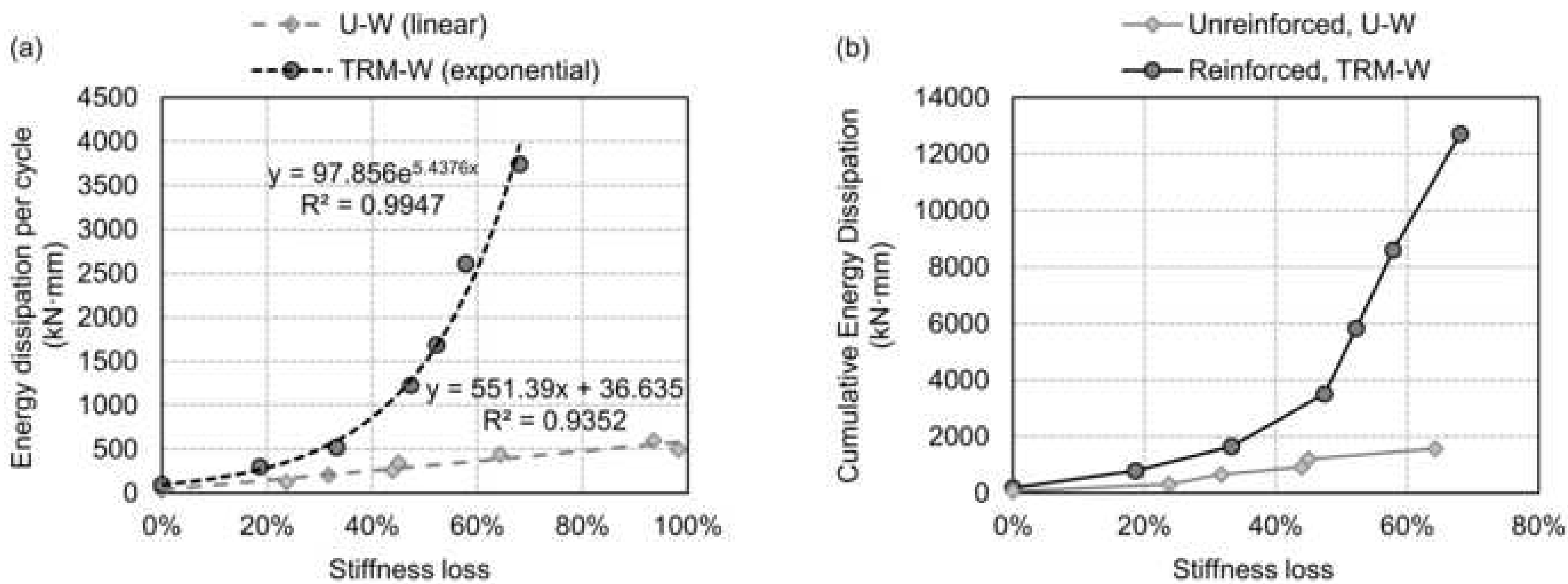
(a)
U-W (linear)
TRM-W (exponential)
y = 97.856e^5.4376x
R² = 0.9947
y = 551.39x + 36.635
R² = 0.9352
Energy dissipation per cycle (kN·mm)
4500
4000
3500
3000
2500
2000
1500
1000
500
0
0%
20%
40%
60%
80%
100%
Stiffness loss
(b)
Unreinforced, U-W
Reinforced, TRM-W
Cumulative Energy Dissipation (kN·mm)
14000
12000
10000
8000
6000
4000
2000
0
0%
20%
40%
60%
80%
Stiffness loss

Figure 10

Click here to access/download;Figure;Fig10.png

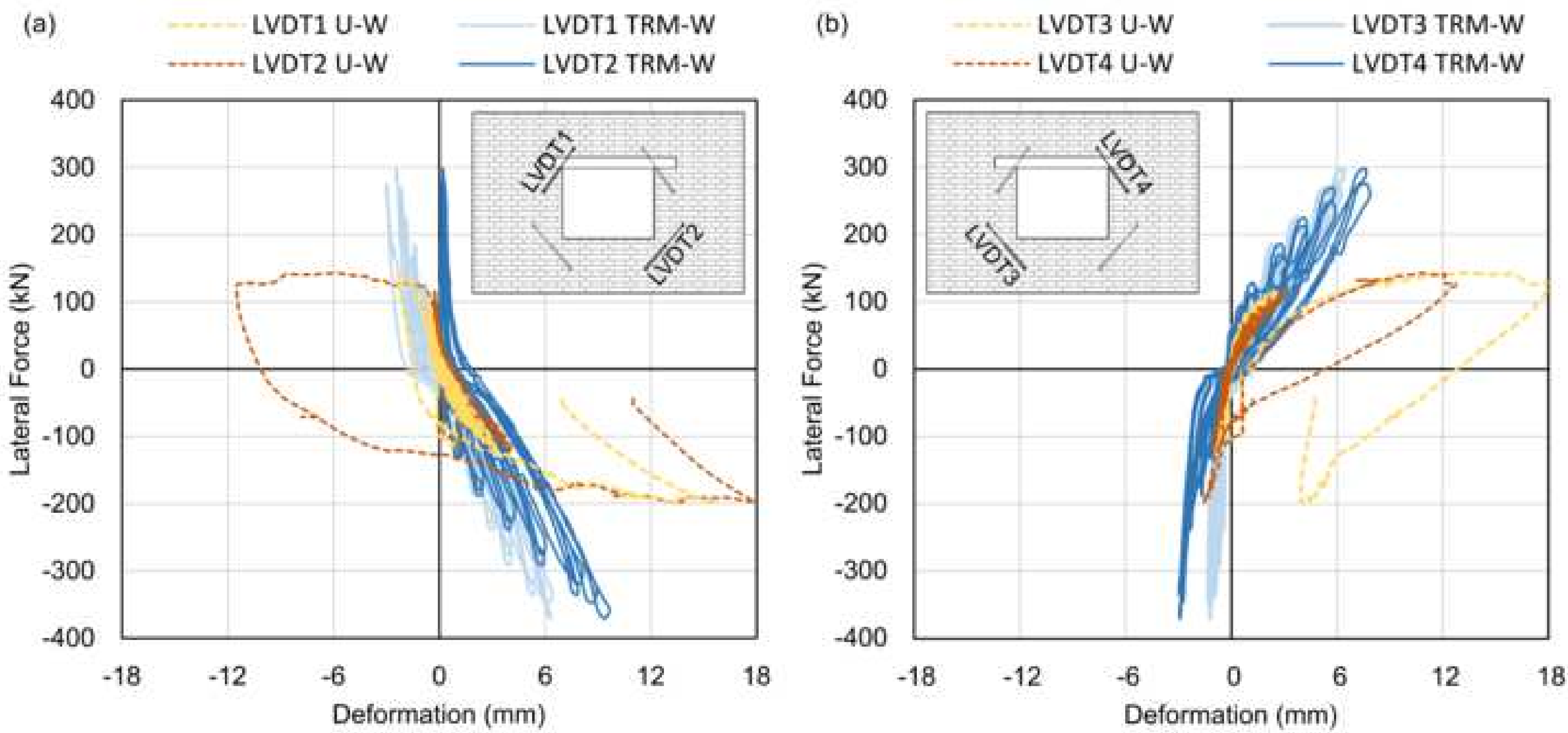

Figure 11

Click here to access/download;Figure;Fig11_v2.tif

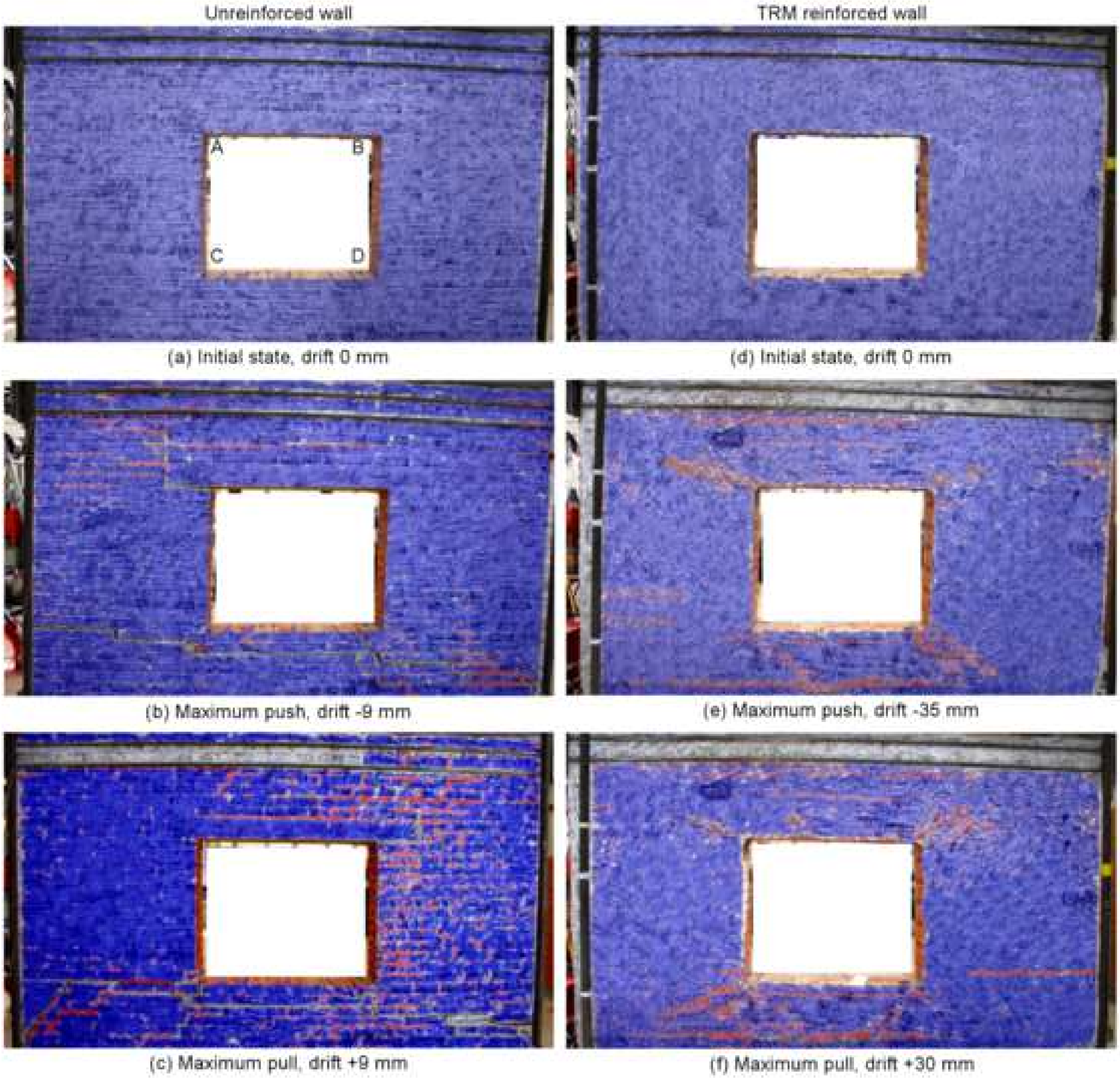

Figure 12

Click here to access/download;Figure;Fig12.tif

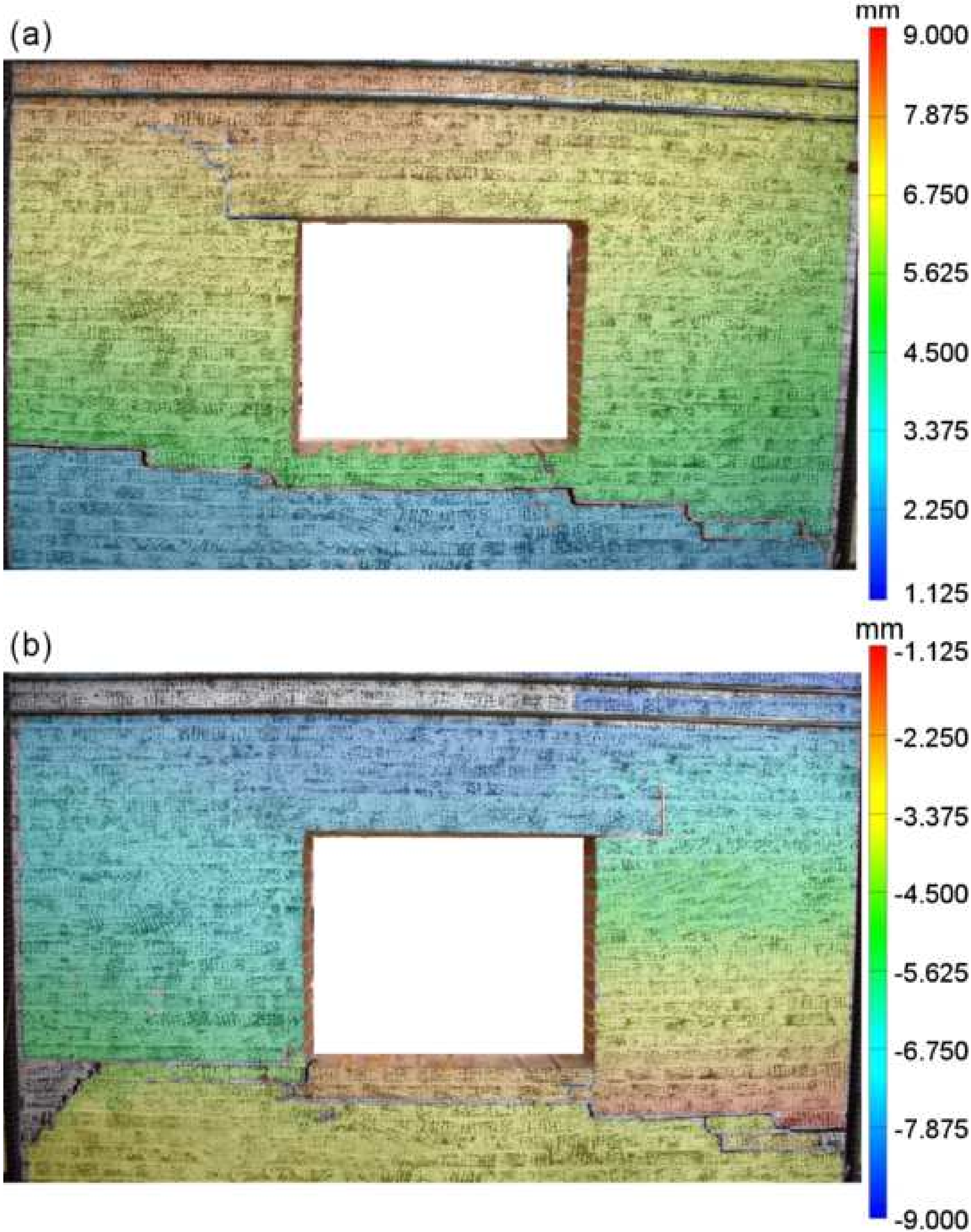

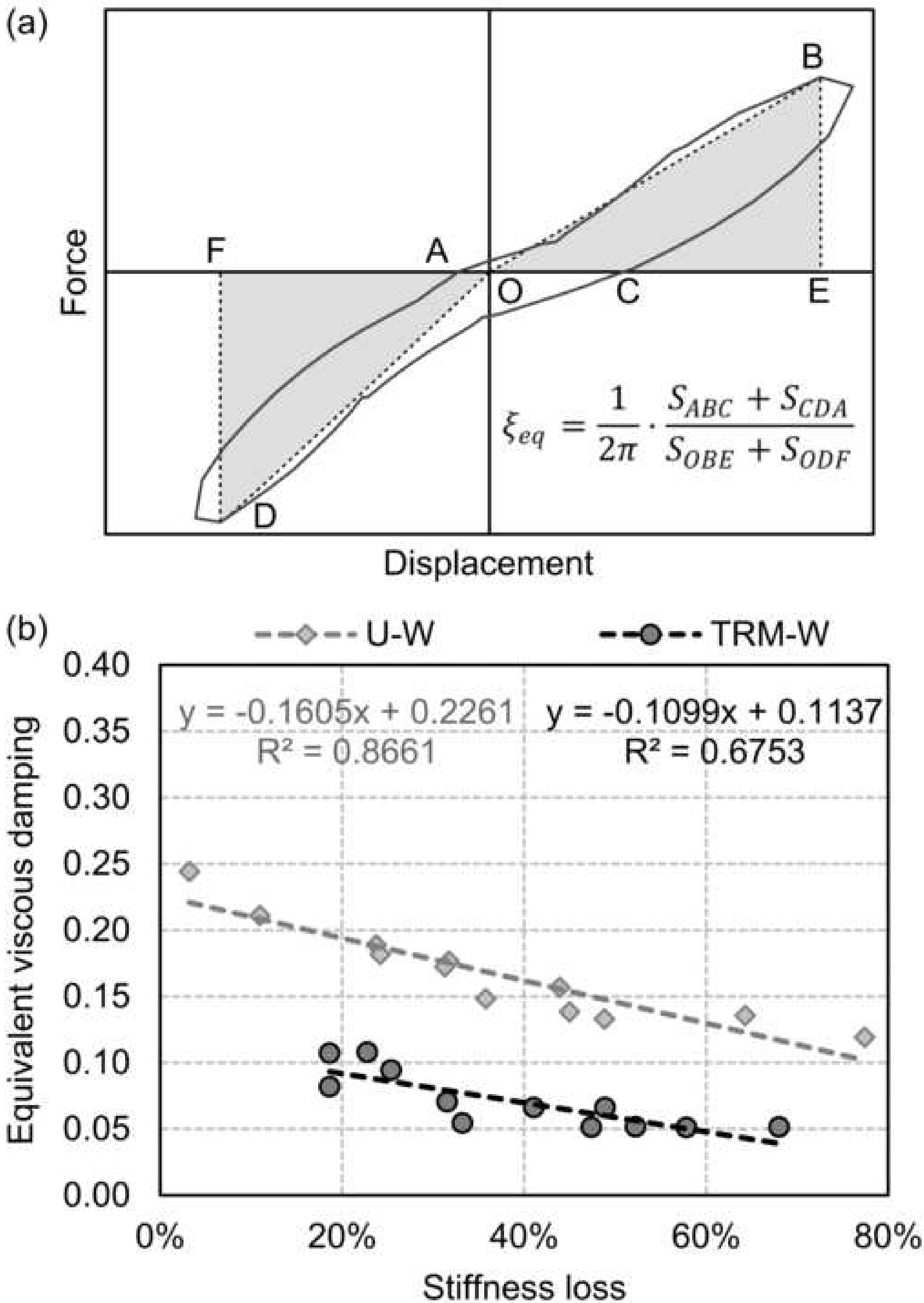
(a)
B
F
A
O
C
E
D
Force
Displacement
$\xi_{eq} = \frac{1}{2\pi} \cdot \frac{S_{ABC} + S_{CDA}}{S_{OBE} + S_{ODF}}$
(b)
U-W
TRM-W
y = -0.1605x + 0.2261
R² = 0.8661
y = -0.1099x + 0.1137
R² = 0.6753
Equivalent viscous damping
0.40
0.35
0.30
0.25
0.20
0.15
0.10
0.05
0.00
0%
20%
40%
60%
80%
Stiffness loss